Journal of Contaminant Hydrology 222 (2019) 31–40

Contents lists available at ScienceDirect

Journal of Contaminant Hydrology

journal homepage: www.elsevier.com/locate/jconhyd

A spatial Markov model for upscaling transport of adsorbing-desorbing solutes

Thomas Sherman[a], Amir Paster[c], Giovanni Porta[b], Diogo Bolster[a,*]

[a] Dept. of Civil and Environmental Engineering and Earth Sciences, University of Notre Dame, IN, USA
[b] Dipartimento di Ingegneria Civile e Ambientale, Politecnico di Milano, Piazza L. Da Vinci, 32, 20133 Milano, Italy
[c] BreezoMeter, Haifa, Israel

ARTICLE INFO

Keywords:
Sorption desorption
Upscaling
Spatial Markov model

ABSTRACT

The Spatial Markov Model (SMM) is an upscaled model with a strong track record in predicting upscaled behavior of conservative solute transport across hydrologic systems. Here we propose an SMM that can account for reactive linear adsorption and desorption processes and test it on a simple benchmark problem: flow and transport through an idealized periodic wavy channel. The methodology is built using trajectories that are obtained from a single high resolution random walk simulation of conservative transport across one periodic element. Our approach encodes information about where a particle starts at the inlet, where it leaves at the outlet, how long it takes to cross the domain and one additional piece of information, the number of times a particle strikes the boundary, with the objective of predicting large scale transport with arbitrary linear adsorption and desorption rates. Our benchmark problem demonstrates that predictions made with our proposed SMM agree favorably with results from direct numerical simulations, which resolve the full transport problem.

1. Introduction

Transport of chemical species through porous media can be complex relative to the flow through the medium due to the fact that constituents can sorb and desorb to the solid matrix, thus slowing down their movement relative to the flow. A common textbook approach to account for this is the inclusion of a retardation coefficient in an advection dispersion equation (ADE) (Bear, 2013). This is only valid when (i) assumptions required to derive the ADE for conservative transport hold and (ii) when one can assume that solute in the fluid and solid phases is in an instantaneous well mixed equilibrium. For complex porous media where geometries can give rise to heterogeneous flows comprised of fast preferential flow channels as well as slower trapping regions, such assumptions can be questionable. Even for conservative transport, where there is no mass exchange between the fluid and the solid phase, anomalous (non-Fickian) transport is known to occur, particularly at early (preasymptotic) times [e.g. (Salles et al., 1992; Lester et al., 2014)]. The problem is further complicated with the addition of potentially complex kinetic surface sorption and desorption processes, which introduce their own set of potentially vastly different time scales (Maghrebi et al., 2014, 2015).

In many instances, it is not of interest to explicitly describe and resolve all details of transport at all scales, but rather model them effectively at some scale of particular interest. Representing the transport of a solute in a complex flow with a one-dimensional upscaled description can be dated back to upscaling transport in cylindrical tubes by GI Taylor and Aris (Taylor, 1953; Aris, 1956); this was later generalized to more complex flow configurations using a variety of related methods [e.g., (Brenner, 1980; Plumb & Whitaker, 1988; Hornung, 1997)]. In all cases, longitudinal transport can be described with an effective one dimensional ADE with an enhanced Fickian dispersion coefficient that reflects spreading due to subscale variations in velocities. These models have been generalized to include a wide variety of reactive processes including surface reactions and mixing processes [e.g. (Shapiro & Brenner, 1988; Dykaar & Kitanidis, 1996; Bolster et al., 2011)]. Dykaar & Kitanidis (1996) calculated effective dispersion, velocity and reaction rates in an idealized pore geometry by considering flow and transport in a periodic channel with sinusoidal boundaries where solute can react and degrade close to the boundaries, a process that is mathematically similar to sorption. Levesque et al. (2012) generalized Taylor dispersion to systems that include adsorption and desorption to and from solid boundaries in the flow domain and applied it to benchmark Poiseuille flows in planar and cylindrical geometries, both in constant and periodic time varying flows. In all cases effective velocities and dispersion coefficients can vary significantly when compared to values obtained for a conservative solute. These

* Corresponding author.
E-mail address: bolster@nd.edu (D. Bolster).

https://doi.org/10.1016/j.jconhyd.2019.02.003
Received 1 November 2018; Received in revised form 31 January 2019; Accepted 4 February 2019
Available online 10 February 2019

coefficients may also vary dynamically in time as recently shown in (Zhang et al., 2017).

The above methods, in their original form, hinge on the assumption that sufficient time has passed for the solute to sample the full variability of flow velocities under displacements induced by diffusion. This is characterized by the Taylor dispersion time scale $\tau_D = L^2/D$, where L is a characteristic length scale and D the diffusion coefficient. At times smaller than this, the aforementioned models are strictly speaking not valid. In the presence of reactions, the relative magnitude of reaction and transport characteristic time scales becomes relevant to the applicability of continuum-scale models, such as the standard advection-dispersion-reaction equation [e.g. (Battiato et al., 2009; Battiato & Tartakovsky, 2011)]. Depending on the nature of the problem at hand, this may or may not be important. For example, many observations of so called anomalous or non-Fickian transport [e.g. (Rehfeldt et al., 1992; Harvey & Gorelick, 2000; Cortis & Berkowitz, 2004)] are situations where all length and velocity scales of the system have not yet been sampled and where the largest time scale might be tremendously large relative to times of practical interest [e.g. (Dentz et al., 2004; Zhang et al., 2007)].

It is possible to relax this assumption and develop similar theories that are valid at pre-asymptotic times [e.g. (Richmond et al., 2013; Porter et al., 2010; Porta et al., 2016)], but these still come with strong assumptions that may or may not be met. A strong benefit of these models is that they can help yield great physical insight into important processes at small scales that dominate large scale behaviors. However, in some instances the resulting models can be highly complex integro-differential equations with strong memory effects, meaning that solving them can be as burdensome as solving the full microscale problem [e.g. (Davit et al., 2012; Porta et al., 2016)].

The Spatial Markov model (SMM), first introduced by (Le Borgne et al., 2008a) provides an alternative, relatively parsimonious approach that can be applied at preasymptotic times, significantly earlier than Taylor dispersion (Sund et al., 2016). The SMM falls into the broad family of continuous time random walk (CTRW) models (Berkowitz et al., 2006). In the SMM, a solute plume is represented as a large number of infinitesimal particles that transition through space and time. Most often, spatial increments are fixed and temporal increments are random, sampled from a measured transition time distribution. This is common to many CTRW models. What sets the SMM apart is that successive temporal increments can be explicitly correlated, reflecting underlying persistence of fast particles to move quickly and slow particles to move slowly, which is particularly important in systems that are advection dominated (Bolster et al., 2014). The SMM has had success in upscaling transport across a diverse set of transport settings, including highly heterogeneous Darcy scale porous media (Le Borgne et al., 2008a; Le Borgne et al., 2008b), fracture networks (Kang et al., 2011), pore scale systems (Le Borgne et al., 2011; De Anna et al., 2013; Bolster et al., 2014; Kang et al., 2014), unsteady flows through porous media (Sund et al., 2015a), and a field scale application to a fractured aquifer (Kang et al., 2015). The model has recently been extended to incorporate nonlinear features such as mixing and reactions (Sund et al., 2015b; Sund et al., 2017a, 2017b). In the above examples, the flows are typically either highly heterogeneous with some random structure, or non-uniform, but with a periodic unit cell, as commonly used in classical upscaling approaches such as volume averaging (Plumb & Whitaker, 1988; Bahar et al., 2018), the method of moments (Brenner, 1980) or homogenization (Hornung, 1997; Boccardo et al., 2018a).

One of the criticisms of the SMM is that it can require extensive parameterization and the most common approach to date is to track Lagrangian particle statistics across two spatial increments, measuring particles transition times across each and representing the correlation structure via a transition matrix. Simplified forms have emerged which assume an idealized structure to the transition matrix and have shown success (Kang et al., 2015; Kang et al., 2016), but the assumed structure may not be sufficiently general to be universal. More recently, an approach was developed that takes successive breakthrough curves and infers the transition matrix structure through an inverse modeling approach (Sherman et al., 2017). This was later applied to laboratory scale data of transport through zeolite packed columns (Sherman et al., 2018). All of these approaches require information about travel times across two spatial intervals. Within a domain composed of periodic cells, Sund et al. (2017b) developed an approach that only requires travel statistics across one cell by parameterizing the model in terms of trajectories rather than just travel times alone. Thus, with one high resolution simulation across one cell (corresponding to one spatial increment in the SMM), they were able to efficiently and rapidly predict large scale transport and mixing across much greater extents, with the upscaled model running on the order of 1000 times faster than a fully resolved one.

The work of (Sund et al., 2017b) was only performed in the context of conservative transport. Here we extend this approach to account for (linear) adsorption and desorption processes. In particular, our goal is to only use trajectory statistics from conservative non-sorbing transport across a single periodic cell to predict larger scale transport of a solute that can adsorb and desorb to the solid matrix with arbitrary adsorption and desorption rates; that is, we only need one high resolution simulation across one periodic element with which to ultimately predict a broad and extensive range of possible transport scenarios across large scales. This extension to sorbing solutes opens the pathways towards the application of this methods to a broad class of reactive transport problems, such as contaminant transport in aquifers (Rathi et al., 2017), as well as flow through membranes and packed bed reactors (Iliev et al., 2017; da Luz et al., 2018). In this work we showcase our modeling procedure by relying on a relatively simple flow geometry. The simplicity of the geometry allows for a clear understanding of emergent behaviors which can then be related to observations in more complex settings. Thus, we regard it as an ideal starting point for our current extension of the SMM. Moreover, a simple geometrical setting can provide critical information with which to parameterize pore network models and therefore help bridge the gap between pore- and continuum-scale [e.g. (Seetha et al., 2014)].

2. Model system

2.1. Pore scale setting

Fig. 1 displays the geometry used in this study, a converging-diverging channel filled with fluid, whose solid boundaries are defined by

$$h(x) = \bar{h} + h' \sin\left(\frac{2\pi x}{L} - \frac{\pi}{2}\right), \tag{1}$$

where x is the horizontal coordinate, $h(x)$, $\bar{h}$ and h' are related to the width of the half-aperture (see Fig. 1), and L is the length of a single cell. In this study, to be consistent with previous ones [e.g. (Sund et al., 2017b; Sund et al., 2015b)], we will focus on the specific values of $\bar{h} = L/4$ and $h' = 0.8\bar{h}$. This setting was first used by (Dykaar & Kitanidis, 1996) to upscale effective reaction rates in porous media using the method of moments. While this geometry is very simple, the emergent flow displays some of the complex features pertinent to understanding flow and transport in porous media, including a fast preferential flow path and stagnant trapping areas, which are known to strongly impact transport in real porous media [e.g. (Edery et al., 2014)]. This, and very similar geometries, have received extensive attention in the literature. For example, (Chaudhary et al., 2013; Chaudhary et al., 2011) and (Bouquain et al., 2012; Bolster et al., 2014) studied the effects of inertia on flow and transport respectively. Similarly, others have looked at how geometry impacts asymptotic (Cardenas, 2009; Bolster et al., 2009) and pre-asymptotic transport (Cardenas, 2008; Le Borgne et al., 2012), as well as the role of turbulence on large scale dispersion (Richmond et al., 2013). One of the reasons we choose this geometry is that under the assumption of Stokes flow, i.e. Reynolds number less than O(1), a semi-analytical solution exists (Kitanidis & Dykaar, 1997; Dykaar & Kitanidis, 1996). The solution uses a perturbation method to solve the biharmonic equation,

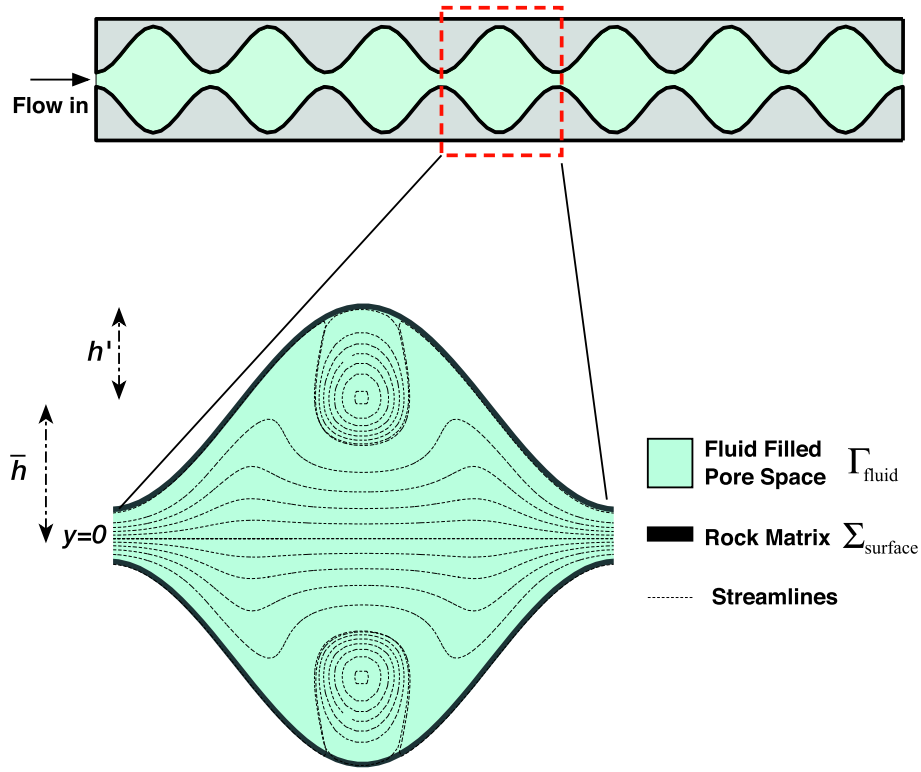

Fig. 1. A schematic of the flow domain and the unit pore cell used in this study.

which governs the streamline structure. Details of the solution, as well as its validation are available in various papers (Kitanidis & Dykaar, 1997; Dykaar & Kitanidis, 1996; Cao & Kitanidis, 1998; Bolster et al., 2009) and so are not elaborated on here. The geometry defined above is chosen because of the interesting flow patterns, including the emergence of a recirculation region and a fast central preferential flow channel. While the geometry is highly idealized, these specific features mimic features of interest in real porous media, making this model potentially appealing. Due to the natural symmetry of the system throughout this entire work we only ever simulate the top half of the domain ($y > 0$).

2.2. Simulation of transport at the microscale

Solute transport with sorption and desorption is modeled by (Khan, 1962; Zhang et al., 2017)

$$\begin{aligned} &\frac{\partial C(\mathbf{x},t)}{\partial t} + \nabla\cdot[\mathbf{u}(\mathbf{x})C(\mathbf{x},t)] = \nabla\cdot[D\nabla C(\mathbf{x},t)] \qquad \forall \quad \mathbf{x}\in\Gamma_{fluid} \\ &\frac{\partial S(\mathbf{x},t)}{\partial t} = -\lambda S(\mathbf{x},t) + \alpha C(\mathbf{x},t) = -D\frac{\partial C}{\partial n} \qquad \forall \quad \mathbf{x}\in\Sigma_{surface} \end{aligned} \tag{2}$$

where $C(\mathbf{x},t)$ $[ML^{-3}]$ is the concentration of the solute in the fluid, $\mathbf{u}(\mathbf{x})$ is the velocity in the fluid phase, D $[L^2T^{-1}]$ is the molecular diffusion coefficient, taken to be constant in the fluid, $S(\mathbf{x},t)$ $[ML^{-2}]$ is the concentration on the surface, λ $[T^{-1}]$ is the rate of desorption, α $[LT^{-1}]$ is the rate of adsorption and n is the unit normal to the boundary. Note that the first equation in (2) describes transport in the main channel, which is governed by the advection diffusion equation. The second equation is the boundary condition, describing exchange between the fluid and solid phase: the rate of change of surface concentration is given by the rate at which solute concentration attaches to the boundary (αC) minus the rate which solid phase concentration is detaching (λS); for mass balance reasons this must be equal to the diffusive flux of solute concentration at the boundary ($-D\frac{\partial C}{\partial n}$). In all cases we consider an initial condition of an instantaneous line source, flux weighted along the pore throat, i.e. $C(\mathbf{x},t=0)\propto\mathbf{u}(\mathbf{x})\delta(x)$. This choice of initial condition is common as it is believed to mimic real experiments [e.g. (Ptak & Teutsch, 1994; Morales et al., 2017)] and also represents the asymptotic distribution to which Lagrangian particles are expected to converge [e.g. (Dentz et al., 2016; Comolli & Dentz, 2017; Kang et al., 2017)].

To solve this system we implement a numerical Lagrangian particle based random walk method (Risken, 1984), where the solute plume is discretized into a finite number of N particles. We incorporate the sorption-desorption boundaries following the work of (Boccardo et al., 2018b). During each step each particle is moved according to Langevin equation

$$\begin{aligned} x_i^{n+1} &= x_i^n + u_i\Delta t + \xi_i\sqrt{2D\Delta t} \\ y_i^{n+1} &= y_i^n + v_i\Delta t + \eta_i\sqrt{2D\Delta t} \qquad i = 1,\ ...,N, \\ t_i^{n+1} &= t_i^n + \Delta t + \tau_i \end{aligned} \tag{3}$$

where x_i^n and y_i^n are the horizontal and vertical position of particle i respectively at simulation step n, u_i and v_i are the x and y components of the velocity respectively, ξ and η are independent and identically distributed (iid) Gaussian variables with zero mean and unit variance, Δt is a fixed time step, t_i^n is the time for particle i at simulation step n, and τ_i is a random waiting time

$$\tau_i = \begin{cases} T_i\text{: } P > U_i \\ 0\text{: } P \le U_i \end{cases}, \tag{4}$$

where the T_i are iid exponential, with density $\psi(\tau) = \lambda\exp[-\lambda\tau]$, P is the probabilty of sorption and U_i are iid $U(0,1)$ (uniformly distributed between 0 and 1). The solid boundaries in the domain are modeled as elastic reflection boundaries. Any time a particle reflects off a solid boundary it either sorbs with probability P, resulting in selecting τ randomly from $\psi(\tau)$, or does not sorb, resulting in $\tau = 0$. To the leading order, this probability can be computed as

$$P = \alpha\sqrt{\frac{\pi\Delta t}{D}}. \tag{5}$$

For further details on this as well as higher order approximations please see (Boccardo et al., 2018b). This number P is compared to a random number U, drawn from a standard uniform distribution. If $U \geq P$ no sorption occurs and if $U < P$ the particle sorbs.

Our choice of solving this system using this Lagrangian random walk method is based on the following: (i) it naturally aligns with building an SMM, which relies on Lagrangian statistics, (ii) for a periodic system like this one, it is possible to simulate very extensive domains as a particle's velocity at any given time depends only on its local position relative to the periodic cell, meaning that we do not need a prohibitively large Eulerian mesh and (iii) for a sufficiently smooth velocity field, such as this one, it is known not to suffer from numerical dispersion, which could be problematic since diffusion and adsorption processes are closely linked. For all of the results that we present in this paper we used one million particles and a time step of $\Delta t = 10^{-3}$, consistent with previous experience in the same domain (Bolster et al., 2009).

2.3. Dimensionless numbers

The system described in Section 2.2 is characterized by the following dimensionless numbers

$$Re = \frac{\bar{h}\bar{u}}{\nu} \qquad Pe = \frac{\bar{h}\bar{u}}{D} \qquad Da_a = \frac{\bar{h}\alpha\sqrt{\pi}}{D} \qquad Da_d = \frac{\bar{h}^2\lambda}{D}. \tag{6}$$

$\bar{u}$ is the mean velocity and ν is the viscosity of the fluid. Re is the Reynolds number, which we have already assumed to be small $Re < O(1)$ in using the prescribed flow field; Pe is the Péclet number, which reflects the competition between advection and diffusion processes and typically lies in the range $0.1 < Pe < 10^3$ (Dykaar & Kitanidis, 1996). We will focus on the higher range of these values, as it is known that advection-dominated systems are more likely to violate assumptions inherent to Taylor dispersion and classical advection-disperison upscaling. Da_a and Da_d are adsorptive and desorptive Damköhler numbers, which respectively compare the time scales associated with adsorptive and desorptive processes to diffusive ones. In a batch system, large values of these would correspond to systems close to equilibrium between surface and fluid concentrations. In the following any reported dimensionless parameters are obtained by setting $\bar{u} = 1$, $2\bar{h} = 1$ (in arbitrary units) and tuning D, α and λ to obtain specified values of Pe, Da_a and Da_d.

2.4. Inputs for spatial Markov model - trajectories, travel times and number of hits

Here we define the inputs that must be obtained from the microscale domain in order to build the macroscale effective SMM, described in the following section. In all cases we obtain these inputs by running a random walk with a flux weighted pulse initial condition at the throat of a pore (see Fig. 1) and simulate transport across one periodic unit cell. This calibration simulation is for a conservative random walk that does not include sorption. The periodic unit cell corresponds to the blown up region in Fig. 1. Sund et al.'s (2017b) SMM is different from others in that it samples trajectories rather than travel times. These trajectories are obtained by simulating transport across a single unit cell, using

$$\begin{aligned} x_i^{n+1} &= x_i^n + u_i\Delta t + \xi_i\sqrt{2D\Delta t} \\ y_i^{n+1} &= y_i^n + v_i\Delta t + \eta_i\sqrt{2D\Delta t} \end{aligned} \qquad i = 1, \ldots, N. \tag{7}$$

This is a standard random walk framework (note these equations are the same as (3), but without the random waiting times associated with modeling sorption). Using this we store specific information about each particle's trajectory. In Sund's approach each trajectory is defined by three parameters: (i) its vertical position at the inlet of the periodic element y_{in}, (ii) the time, T, it takes to travel from the inlet to the outlet and (iii) its vertical position at the outlet when it leaves the periodic element y_{out}. In addition to these three inputs, our method will account for adsorption-desorption by storing one additional piece of information (iv) N_{hits}, the number of times a particle strikes a solid boundary when crossing a single cell. We propose that by running one high resolution simulation of conservative transport over one periodic element, we can obtain all of the required information needed to upscale and describe transport with adsorption and desorption efficiently over much larger scales. However, it must be noted that for each different value of Pe, a different calibration simulation is required.

2.5. Effective transport model - the spatial Markov model

Here we propose an SMM, which is an effective upscaled transport model that describes transport in one dimension aligned with the direction of flow. The SMM is a time domain random walk model and again the solute is represented by discrete particles, whose motion in time and space is governed by:

$$\begin{aligned} \tilde{x}_i^{k+1} &= \tilde{x}_i^k + L \\ \tilde{t}_i^{k+1} &= \tilde{t}_i^k + T_i^k + \sum_{j=1}^{N_{hits}^k} \tau_j. \end{aligned} \tag{8}$$

Tildes refer to upscaled quantities. $\tilde{x}_i^k$ is the horizontal location of particle i at the beginning of step k, $\tilde{t}_i^k$ is the time associated with particle i at the beginning of step k, N_{hits}^k is the number of times the sampled trajectory strikes the boundary during step k. During each step a particle transitions a constant longitudinal distance L, the length of our periodic cell, and it does so in a random time T, which is sampled from a measured travel time distribution, the discrete distribution obtained from the single pore calibration simulation in (7). T reflects the range of velocities that particles sample in traversing the unit cell. The feature that makes the SMM unique relative to other random walk models is that successive temporal increments are not independent of one another. Correlation arises when a particle that traverses one periodic unit quickly is also likely to traverse the next one quickly and likewise for a slow one. In the absence of diffusion, particles persist on the same streamline always and so successive jumps would have the same transition time. Due to diffusion, particles can leave streamlines and sample various flow streamlines. However, when advective effects are strong relative to diffusive ones, memory effects persist and must be accounted for through correlation. In most applications, correlations are applied using a transition matrix (Le Borgne et al., 2008a). We apply here instead the trajectory based approach recently proposed in (Sund et al., 2017b), because the trajectory based method can account for the number of times each trajectory interacts with the boundary in a way that the original transition matrix approach cannot. This approach naturally provides a framework that more readily characterizes interactions of particles with the reactive boundary, using the information stored as inputs for the SMM described in §2.4. It should be noted that the periodic nature of the domain is important in accomplishing this, although some other recent studies suggest that trajectory based methods may also work for heterogeneous systems characterized by a stationary heterogeneity distribution (Wright et al., 2019; Most, 2019).

In this implementation of the model, each step of length L is associated with a specific particle trajectory. We summarize our algorithm in the following steps:

1. Each particle starts with a given y_{in} reflecting the desired initial condition. This sets a specific trajectory that has an associated travel time, which is used as the time increment T_i^k in (8), and an assigned number of hits ${N_{hits}}^k$.
2. Adsorption is accounted for by the term $\sum_{j=1}^{N_{hits}^k} \tau_j$, where each strike with the boundary adds a possible waiting time, which is sampled from the same distribution $\psi(\tau)$ as used in (3) with probability P from (5).
3. The model then samples the next trajectory randomly, using y_{out} as a conditioning criterion for picking the next trajectory by making sure

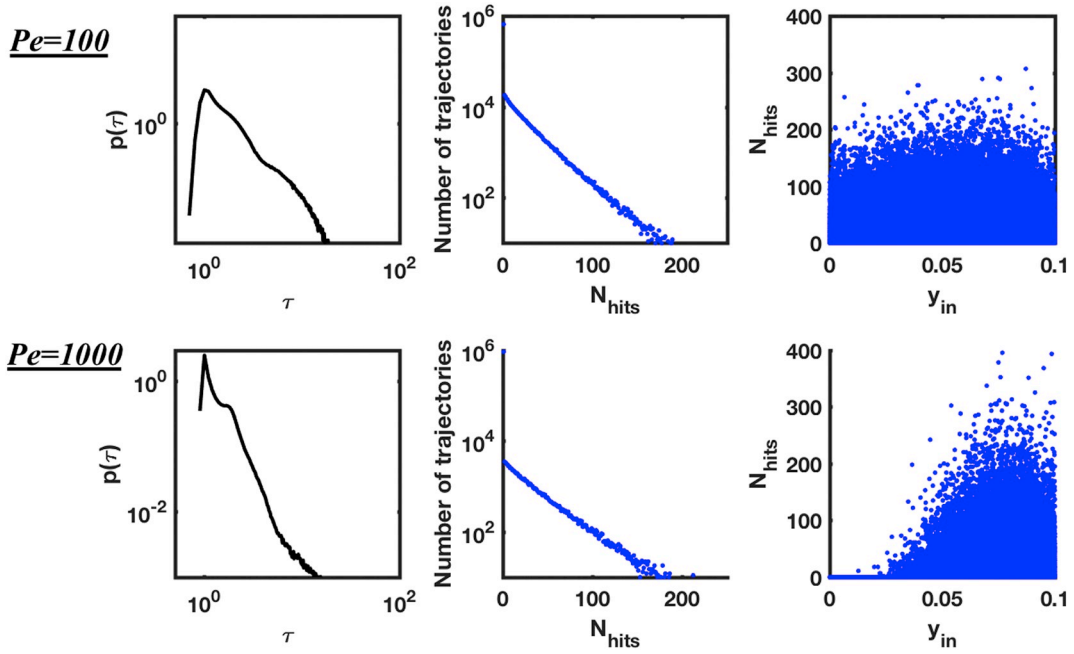

Fig. 2. (Left) Travel Times Distributions across single periodic elements (Middle); Frequency scatter plot of number of times each trajectory hit the boundary; (Right) Scatter plot for each simulated particle's starting y_{in} vs the number of times a particle hits the boundary during one travel time. The top row shows results for $Pe = 100$ and the bottom row for $Pe = 1000$.

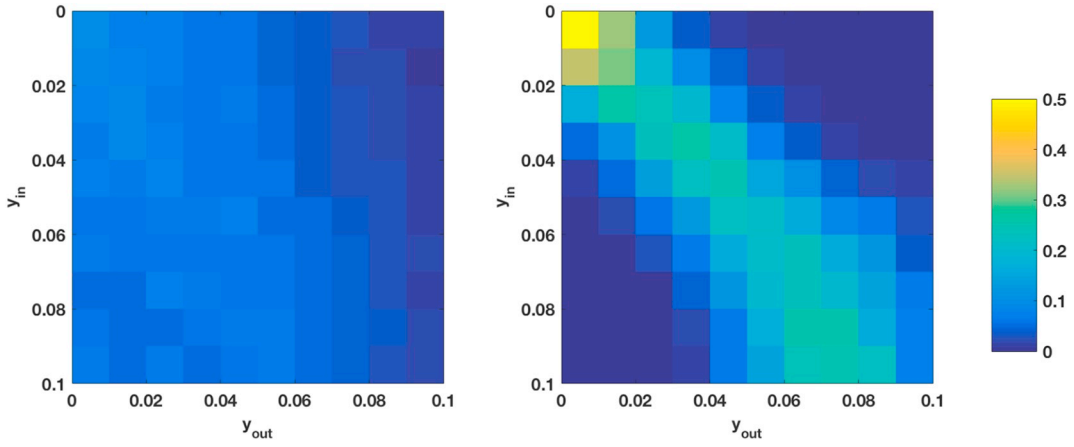

Fig. 3. Transition probabilities of y_{out} given y_{in} for $Pe = 100$ (left) and $Pe = 1000$ (right). In this figure y_{in} and y_{out} are discretized into 10 bins of equal size.

that its y_{in} is close to the previous y_{out}. This is done by discretizing the inlet into N_{bins} equi-sized bins (we used cases with $N_{bins} = 10$, 100 and 1000 in this study with no notable difference in results). A particle's vertical y location determines which bin it is in. Thus y_{out}^k determines the bin from which the next trajectory is sampled. A trajectory with y_{in}^{k+1} is randomly and uniformly sampled from the same bin that y_{out}^k ends in. This binning procedure ensures correlation effects are accurately imposed.

2.6. Observables to test model

We will test the proposed SMM by comparing its ability to predict downstream transport as measured by breakthrough curves (BTCs) measured at multiple downstream locations. These are $x = 5L$, $10L$, $25L$ and $50L$. Testing the upscaled model against BTCs at multiple downstream locations provides a more robust test of the model compared with focusing on only one location; sometimes a model can match a single BTC due to overparameterization, but when the same model can consistently match observations over multiple scales, it suggests that the underlying physics is being more faithfully captured. Thus, to produce benchmark data against which to test the SMM, we run a series of high resolution random walk simulations using the fully resolved transport Eq. (3) that account for advection, diffusion, adsorption and desorption. In all cases we use a flux weighted pulse initial condition and run single realization simulations with $N = 10^6$ particles. These results are the reference solution against which the upscaled model is tested.

3. Results

3.1. Travel time distributions and number of hits

Fig. 2 displays the empirical travel time distributions, measured from simulations, across a single periodic element for two cases, $Pe = 100$ and $Pe = 1000$. The data used to plot these travel time distributions is from where temporal increments are sampled. These two Péclet numbers are chosen because, in the case of purely conservative transport, it has been shown that for $Pe = 100$ incorporating correlation effects is unimportant, while for $Pe = 1000$ it is (Bolster et al., 2014). These distributions were obtained by creating a histogram of arrival times and normalizing. The bin size of the histogram grew logarithmically with larger τ.

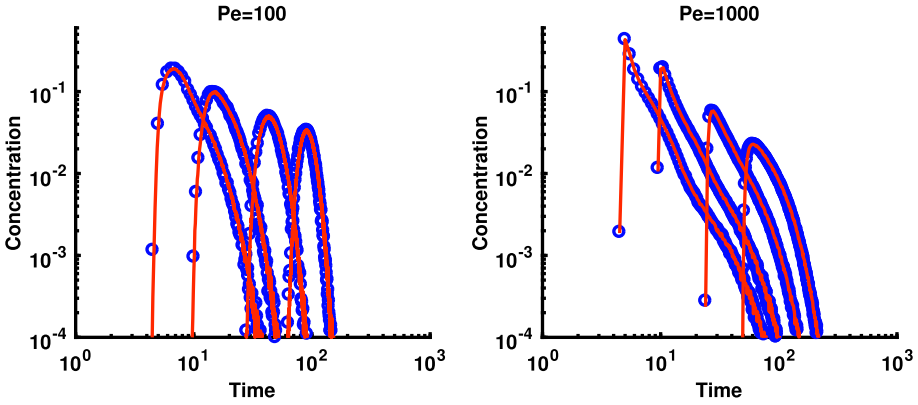

Fig. 4. Breakthrough Curves for $Pe = 100$ (left) and $Pe = 1000$ (right) at distances of $5L$, $10L$, $25L$ and $50L$ with no sorption at all. Blue dots are DNS results and black lines are SMM predictions. (For interpretation of the references to colour in this figure legend, the reader is referred to the web version of this article.)

Also shown are the number of times a particle (trajectory) strikes the boundary during a given transition across a single cell. Most notably, for both Péclet numbers the vast majority (approximately 99%) of trajectories never actually strike the boundary and pass through the pore with no possibility of adsorption taking place. However, some trajectories can strike the boundary anywhere up to 200 times, meaning that the likelihood of adsorption can be significant depending on the adsorption rate, or the probability of attachment P. For the lower Péclet number case more trajectories strike the boundary than in the $Pe = 1000$ case, which intuitively makes sense given that the surface reaction is diffusion-driven. The expected delay for a reactive particle that strikes the boundary N_{hits} times is $\langle\tau\rangle = \frac{N_{hits}P}{\lambda}$, where the angled brackets denote the expected value.

Finally, Fig. 2 shows a scatter plot of each simulated trajectory's starting location at the inlet against the number of interactions with the boundary. This figure clearly highlights that for the $Pe = 1000$ case a particle has to start near the boundary in order to have any chance of interacting with it. A particle that starts on the centerline $y = 0$ has nearly zero likelihood of interacting with the boundary and thus adsorbing. For the $Pe = 100$ case, the number of hits per trajectory is relatively independent of y_{in}. This suggests that accounting for correlation effects (i.e. knowing a particle's starting location as it transitions through each pore) may be less important for $Pe = 100$ than for $Pe = 1000$, as found in the conservative case (Bolster et al., 2014).

Fig. 3 displays the discrete transition probabilities that a particle has for a y_{out} given a particular y_{in}, which is a measure of correlation. Note that this figure is an approximation of the copula density function defining correlation between travel times in consecutive steps (Massoudieh et al., 2017). As has been seen in previous studies for $Pe = 100$, this matrix is relatively uniform, while there is a stronger diagonal dominance for the $Pe = 1000$ case reflecting the fact that correlation effects become stronger as Péclet number increases (Bolster et al., 2014).

3.2. Comparison between DNS and SMM predicted breakthrough curves

3.2.1. Limit of no sorption ($P = 0$)

To begin, we demonstrate the proposed SMM's ability to upscale transport in the absence of any sorption at all. Plots comparing breakthrough curves at multiple downstream locations measured by DNS and predicted with the SMM are shown in Fig. 4. As in previous studies, the agreement is excellent demonstrating the veracity of our proposed approach.

3.3. Limit of unit probability

Next we focus on another limiting case, where the probability of sorption each time a particle strikes the boundary is unity ($P = 1$), meaning that every strike results in an adsorption event. While this may not be an entirely physical condition, by considering this extreme case we are testing our proposed procedure across a wide range of possible Da_a. For $Pe = 100$ and $Pe = 1000$ the respective values are $Da_a = 316$ and $Da_a = 10^3$. The considered values of $\lambda = 0.1$ and 1 correspond to $Da_d = 10$, 10^2 and $Da_d = 10^2$, 10^3 respectively.

Results comparing DNS measured breakthrough curves as well as SMM predicted ones are shown in Fig. 5. Additionally, for context and to explicitly demonstrate the role of sorption, breakthrough curves for the case of zero sorption, as discussed in the previous section, are also included. Again, the agreement between DNS and SMM is excellent, with the SMM capturing all essential features displayed by the fully resolved simulations.

For the $Pe = 100$ case the rising limb of the two earlier breakthrough curves is similar for the cases with and without sorption. This corresponds to fast moving particles following trajectories that never interact with the boundary. The late time behavior and the further downstream breakthrough curves are very distinct with a strong separation between the case with and without sorption, reflecting strong delays due to sorption. For the $Pe = 1000$ case more particles persist at moving quickly and do not interact with the boundary; thus the early arrivals are similar between cases with and without sorption. Again, at late times there is a deviation between the cases with strong delays in the tails emerging for the cases with sorption.

3.4. Intermediate sorption

Results corresponding to a sorbing probability that is one order of magnitude smaller than in the previous section, $P = 0.1$, are shown in Fig. 6, which correspond to $Da_a = 31.6$ and 100. The results demonstrate that the SMM provides reliable results across the parameter space.

The resulting breakthrough curves reflect very similar behavior to the previous case; however the tails are not as delayed, reflecting the fact that only 10% of particles that sorbed in the $P = 1$ case actually do so here. For the $Pe = 1000$ and $Da_d = 1000$ case ($\lambda = 1$, Fig. 6 top right), it is visually next to impossible to see differences at late times, while for the longer waiting time $Da_d = 100$ ($\lambda = 0.1$, Fig. 6 bottom right) a more distinct delayed tailing behavior emerges for the cases with sorption. Note that breakthrough curves obtained with $P = 0.1$, $\lambda = 0.1$ (bottom row in Fig. 5) are identical to the ones for $P = 1, \lambda = 1$ case (top row in Fig. 4) because their expected delay times are equivalent. This is because, on average, multiplying both P and λ by a constant has no effect on average travel times.

3.5. The role of correlation

In this section, we test how important including correlation in the SMM is for accurately predicting downstream reactive transport behavior. To do so, an uncorrelated one-dimensional time domain random

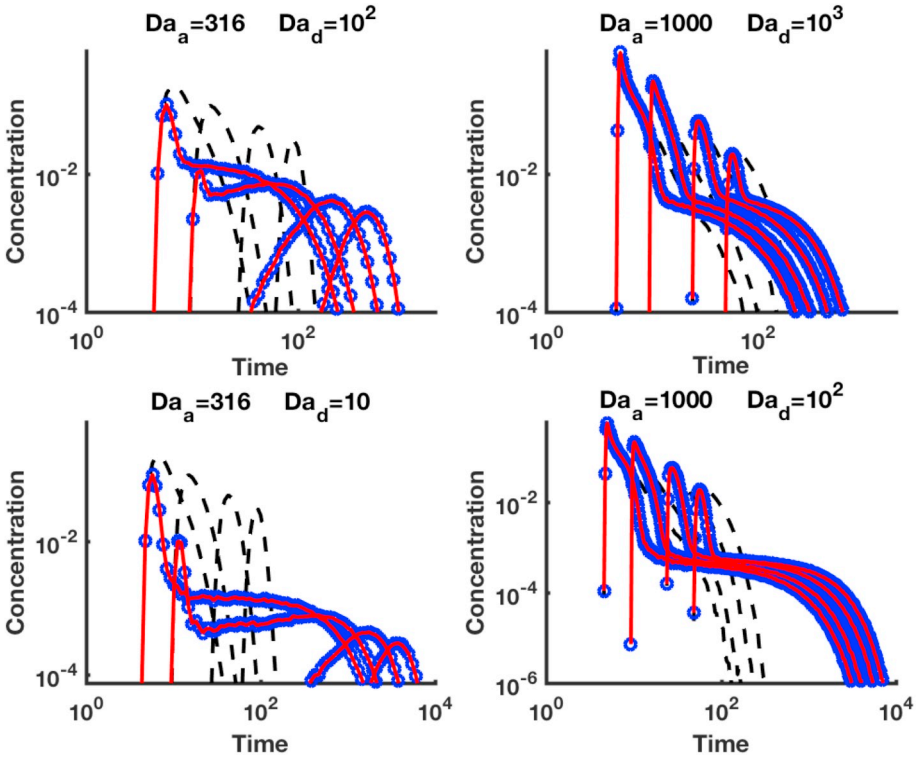

Fig. 5. Breakthrough Curves for $Pe = 100$ (left) and $Pe = 1000$ (right) at distances of $5L$, $10L$, $25L$ and $50L$ with sorption given by $P = 1$. Blue dots are DNS results and red lines are SMM predictions. Black dash-dot lines are BTCs for the case without sorption. (For interpretation of the references to colour in this figure legend, the reader is referred to the web version of this article.)

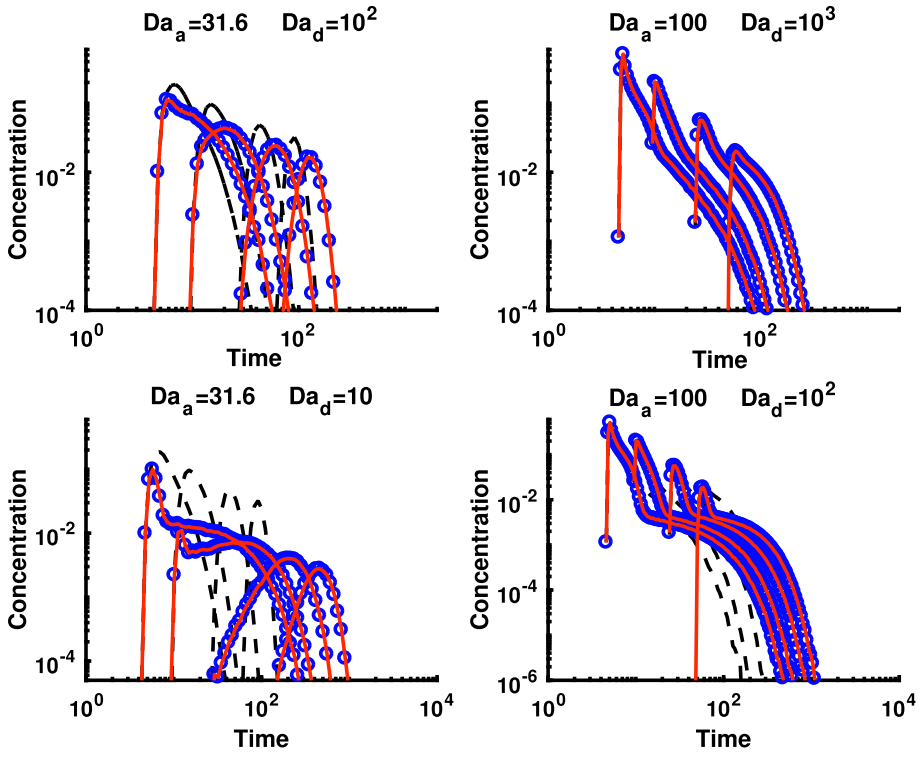

Fig. 6. Breakthrough Curves for $Pe = 100$ (left) and $Pe = 1000$ (right) at distances of $5L$, $10L$, $25L$ and $50L$ with sorption given by $P = 0.1$. Blue dots are DNS results and red lines are SMM predictions. Black dash-dot lines are BTCs for the case without sorption. (For interpretation of the references to colour in this figure legend, the reader is referred to the web version of this article.)

walk (TDRW) model is built by simply sampling random trajectories without considering the inlet and outlet locations, which are the quantities by which we enforce correlation in our model. The trajectories are sampled uniformly from the calibration simulation data.

Fig. 7 shows the comparisons for all parameter choices considered so far, but focusing only the furthest downstream BTC ($x = 50L$). As expected, the importance of correlation effects is stronger for the $Pe = 1000$ cases than for $Pe = 100$. However, even for $Pe = 100$ distinguishable errors are visible where successive travel times are sampled independently. This suggests that, while correlation effects are seemingly unimportant for the $Pe = 100$ case for conservative transport (Bolster et al., 2014), as sorption at the boundary occurs, correlation begins to play some role, similar to what has been observed for reactions (Sund et al., 2015b).

Notably, when correlation is not accounted for, predicted breakthrough curves fail to capture the full rising limbs and also display greater delays than the actual measured ones. This reflects the fact that

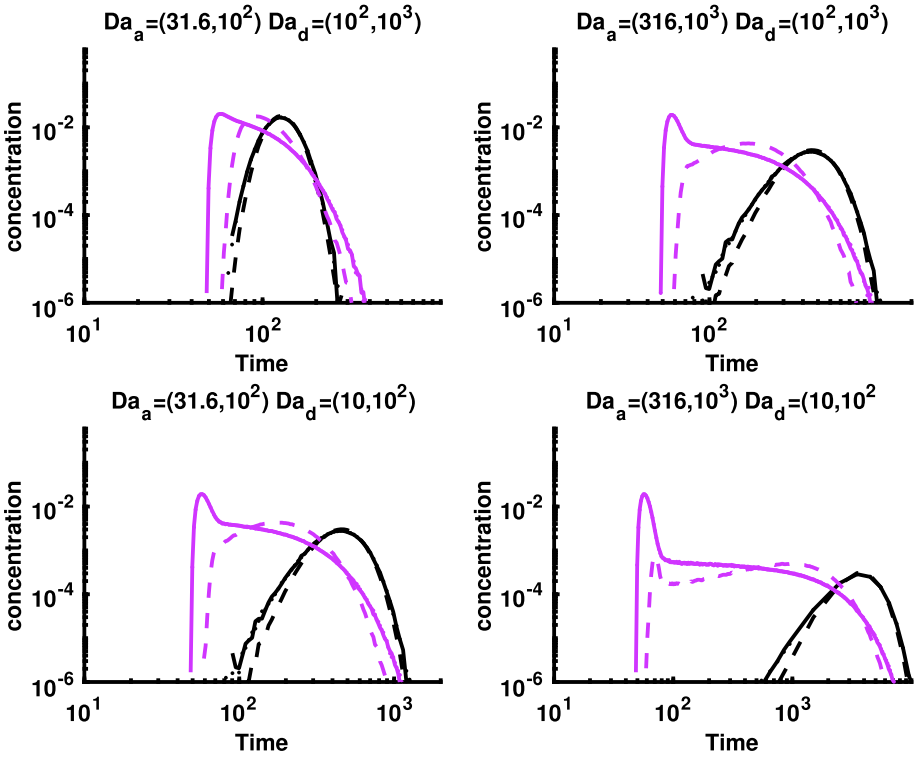

Fig. 7. Breakthrough curves at a distance of 50*L* for $Pe = 100$ (black) and $Pe = 1000$ (magenta). Solid lines are the SMM with correlation effects included, while dashed lines do not include correlation effects. Dots are results from the DNS simulations (note that these are hard to see as they coincide so closely with the SMM results). Damköhler numbers in parentheses are for $Pe = 100$ and 1000 respectively. (For interpretation of the references to colour in this figure legend, the reader is referred to the web version of this article.)

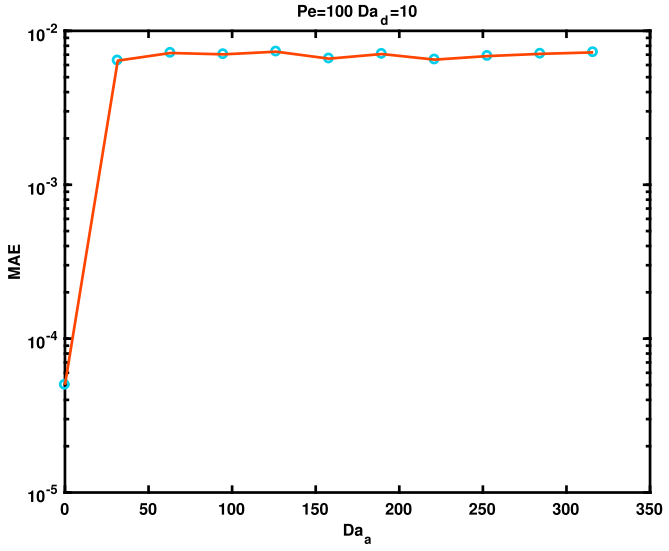

Fig. 8. Mean absolute error (MAE) between recovered mass simulated by direct numerical simulation and uncorrelated simulations at 50*L*, for $Pe = 100$ and $Da_d = 10$ as a function of Da_a.

too many particles are interacting with the boundary. The uncorrelated model cannot account for the fact that fast particles have a tendency to persist at staying fast, as well as the fact that the fastest particles have virtually no probability of getting sorbed, as shown in Fig. 2.

While well known that correlation plays an ever more important role as the Péclet number of a system increases, the effect of boundary reactions on the importance of correlations between successive jumps has not been previously explored. Fig. 8 quantifies this effect based on the approximation of particle arrival times. More specifically, we consider the recovered mass at time t

$$M(t) = \int_0^t C(x = 50L, t')dt' \tag{9}$$

which is the cumulative distribution function of solute arrival times at $x = 50L$. We compute the mean absolute error ($MAE = \Sigma_{i=1}^{N_t} |M_{DNS}(t_i) - M_{simulated}(t_i)|$) between the results obtained via DNS and the upscaled simulation with uncorrelated steps at location 50*L*. Our results, in agreement with previous studies, show that the uncorrelated model can yield accurate arrival times of a nonreactive solute ($Da_a = 0$) for $Pe = 100$ as the MAE attains a value of $\sim 5 \times 10^{-5}$. The occurrence of adsorption induces an increase of the MAE by approximately two orders of magnitude, irrespective of the probability with which reaction occurs. This is likely because only slower particles ever interact with the boundary and, while weak, some correlation does occur. This does not mean that the model is not sensitive to *P*; indeed it must be since larger values of *P* result in larger delays. It is only saying that correlation effects may be more important to include in the upscaled model when sorption occurs. Note that when correlation is included the MAE is approximately constant for all adsorption probabilities (including the conservative case, $P = 0$) and attains a value of approximately 10^{-5} (not shown).

Additionally, to provide another basis for comparison, Table 1 shows the arrival times when 1%, 50% and 99% of the mass has arrived for all of the cases shown in Fig. 7. We show the dimensionless time for DNS and the relative difference R_Δ between DNS and the two models, computed as

$$R_\Delta(MOD) = \frac{t_{pc}(MOD) - t_{pc}(DNS)}{t_{pc}(DNS)} \tag{10}$$

where *MOD* stands for UNC (uncorrelated TDRW) or SMM and t_{pc} indicates the time corresponding to arrivals of percentile *pc* of total mass (i.e., *pc* equals 1%, 50% and 99% here). These results clearly and quantitatively highlight the good agreement between the DNS and SMM as well as the aforementioned discrepancies between the DNS and uncorrelated TDRW model. Differences between DNS and SMM are always within 1%, showing the robustness of the method. On the other hand, when correlations are neglected, the errors increase sharply with *Pe*, i.e. relative differences between uncorrelated model and DNS are up to 10–15% for $Pe = 100$ and up to 90% for $Pe = 1000$. In general, the

Table 1
Arrival times for 1, 50, and 99% of the solute plume to cross 50L in the DNS and relative difference R_Δ related to the upscaled SMM, and uncorrelated TRDW (UNC). Cases correspond to different combinations of adsorptive and desorptive Damköhler numbers.

	$Pe = 100$								
Case	1% arrival time			50% arrival time			99% arrival time		
	DNS	$R_\Delta(SMM)$	$R_\Delta(UNC)$	DNS	$R_\Delta(SMM)$	$R_\Delta(UNC)$	DNS	$R_\Delta(SMM)$	$R_\Delta(UNC)$
$Da_a = 31.6$, $Da_d = 10$	208.5	0.58%	11.68%	478.5	0.31%	0.71%	888.4	−0.14%	−3.82%
$Da_a = 31.6$, $Da_d = 100$	85.9	0.23%	5.34%	130.9	0.15%	0.46%	198.9	−0.30%	−2.72%
$Da_a = 316$, $Da_d = 10$	1416.8	0.77%	15.09%	3953.1	0.40%	0.73%	7800.7	0.21%	0.73%
$Da_a = 316$, $Da_d = 100$	208.6	0.48%	11.78%	478.7	0.21%	0.73%	886.6	0.00%	−3.46%
				$Pe = 1000$					
$Da_a = 100$, $Da_d = 100$	52.3	0.19%	42.94%	139.8	0.50%	52.46%	635.1	0.60%	−13.35%
$Da_a = 100$, $Da_d = 1000$	52.3	0.19%	34.73%	84.4	0.36%	23,26%	219.7	0.59%	−10.18%
$Da_a = 1000$, $Da_d = 100$	52.3	0.00%	76.77%	675.2	1.13%	89.84%	4911.7	1.09%	−12.92%
$Da_a = 1000$, $Da_d = 1000$	52.3	0.00%	42.83%	139.9	0.43%	52.60%	635.1	0.60%	−13.35%

uncorrelated TDRW overestimates early arrivals and underestimates late arrivals. Correlation effects also appear to have different influence depending on Da_a and Da_d. These differences emerge in the 1% and 50% arrival times (early arrivals and median time), although with relatively smaller variations than the ones observed for Pe. For early arrivals and median time, the uncorrelated model errors tend to increase for increasing Da_a and decrease with increasing Da_d, i.e. the error may change up to a factor 2 when the two Damköhler numbers change by one order of magnitude.

4. Discussion and conclusions

We have extended the Spatial Markov Model for periodic flow domains proposed in (Sund et al., 2017b) to account for linear adsorption to and desorption from solid boundaries. In particular, we have built the framework based on a trajectory based SMM, where high resolution trajectories simulated by an advective-diffusive random walk over a single periodic flow element are stitched together sequentially to predict transport over much larger scales. In this novel approach we merely store one additional piece of information about each trajectory, that is the number of times that it strikes a solid boundary. This information reflects the solute flux close to the boundary surface that corresponds to the adsorption reaction rate. Coupling this with a probabilistic representation of sorption (Boccardo et al., 2018b), we can effectively upscale transport to represent arbitrary adsorption and desorption rates. Thus, from a single high resolution random walk simulation of conservative transport across one periodic element, we can model an extremely diverse range of adsorption/desorption behaviors without the need to run further high resolution, computationally intensive, small scale simulations for each desired case. Of course, this current application is strictly restricted to the example of an idealized periodic setting and it remains to be shown how generalizable it is to more complex and realistic settings.

As in previous studies of conservative transport, the need for the upscaled model to account for correlation between successive jumps depends on the Péclet number of the system, with correlation being more important as advection begins to dominate more and more. Similarly, it appears that the Damköhler numbers play a role in determining how important correlation is; merely delineating regions where correlation is important or unimportant for conservative transport does not provide a sufficient condition for the case when reaction occurs. This is particularly relevant for the accurate representation of early and late particle arrivals with the upscaled model, because these are most sensitive to correlation effects (fast particles tend to persist as fast and slow as slow). For the conditions explored, we have numerically verified that the correlation between subsequent travel times plays a relevant role across the full range of investigated adsorption rates. As expected, the relevance of correlation is sharply influenced by Pe, but also increases with Da_a (fast adsorption) and decreases with Da_d (fast desorption). This trend is particularly striking for early arrivals, which could be of practical relevance, e.g., in assessment of membranes lifecycle or of risk with contaminant breakthrough in aquifers. Notably, our approach conserves the same accuracy with respect to fully resolved simulations for both conservative and reactive transport.

Our model can accurately upscale kinetic sorption and desorption processes, i.e. it does not assume equilibrium between sorbed and dissolved solute mass, as would be the case if modeling adsorption/desorption with a retardation coefficient. We emphasize that the traditional use of a retardation factor to account for the delays in transport induced by adsorption and desorption will not work to reproduce the cases that we simulate here. The main effect of a retardation coefficient would simply be a rescaling in time of a conservative concentration profile or breakthrough curve. However, the breakthrough curves obtained in this study, in many cases, have a fundamentally different shape from those without adsorption and desorption. The use of a retardation coefficient assumes an instantaneous equilibrium between mobile and immobile parts of the domain and clearly that is not the case here, particularly for the higher Péclet number case. The persistence of correlation effects is very much inline with the fact that highly mobile particles traveling on fast trajectories have virtually no interaction with the boundaries while slower ones can have many, reflecting a lack of equilibrium. As with upscaling of other transport processes, at late times as systems begin to homogenize (i.e. greater than Taylor time scales) conditions for such an equilibrium can arise, but this may or may not be useful depending on the scales that one is interested in.

Acknowledgments

This material is based upon work supported by, or in part by, the US Army Research Office under Contract/Grant number W911NF-18-1-0338. The authors were also supported by the National Science Foundation under awards EAR-1351623 and EAR-1417264, EAR-1446236, and CBET-1705770.

References

Aris, R., 1956. On the dispersion of solute in a fluid flowing through a tube. Proc. R. Soc. Lond. Ser. A 235, 67–77.
Bahar, T., Golfier, F., Oltean, C., Lefevre, E., Lorgeoux, C., 2018. Comparison of theory and experiment for napl dissolution in porous media. J. Contam. Hydrol. 211, 49–64. https://doi.org/10.1016/j.jconhyd.2018.03.004.
Battiato, I., Tartakovsky, D., 2011. Applicability regimes for macroscopic models of reactive transport in porous media. J. Contam. Hydrol. 120, 18–26.
Battiato, I., Tartakovsky, D.M., Tartakovsky, A.M., Scheibe, T., 2009. On breakdown of macroscopic models of mixing-controlled heterogeneous reactions in porous media. Adv. Water Resour. 32 (11), 1664–1673.
Bear, J., 2013. Dynamics of Fluids in Porous Media, Courier Corporation.
Berkowitz, B., Cortis, A., Dentz, M., Scher, H., 2006. Modeling non-Fickian transport in geological formations as a continuous time random walk. Rev. Geophys. 44 (2).
Boccardo, G., Crevacore, E., Sethi, R., Icardi, M., 2018a. A robust upscaling of the effective particle deposition rate in porous media. J. Contam. Hydrol. 212, 3–13.

https://doi.org/10.1016/j.jconhyd.2017.09.002.
Boccardo, G., Sokolov, I.M., Paster, A., 2018b. An improved scheme for a robin boundary condition in discrete-time random walk algorithms. J. Comput. Phys. 374, 1152–1165.
Bolster, D., Borgne, T.L., Dentz, M., 2009. Solute dispersion in channels with periodically varying apertures. Phys. Fluids 21, 056601.
Bolster, D., Valdes-Parada, F., Borgne, T.L., Dentz, M., Carrera, J., 2011. Mixing in confined stratified aquifers. J. Contam. Hydrol. 120–121, 198–212.
Bolster, D., Méheust, Y., Le Borgne, T., Bouquain, J., Davy, P., 2014. Modeling preasymptotic transport in flows with significant inertial and trapping effects–the importance of velocity correlations and a spatial Markov model. Adv. Water Resour. 70, 89–103.
Bouquain, J., Meheust, Y., Bolster, D., Davy, P., 2012. The impact of inertial effects on solute dispersion in a channel with periodically varying aperture. Phys. Fluids 24, 083602.
Brenner, H., 1980. Dispersion resulting from flow through spatially periodic porous media. Philos. Trans. R. Soc. Lond. A 297, 81–133.
Cao, J., Kitanidis, P., 1998. Adaptive finite element simulation of stokes flow in porous media. Adv. Water Resour. 22 (1), 17–31.
Cardenas, M.B., 2009. Direct simulation of pore level Fickian dispersion scale for transport through dense cubic packed spheres with vortices. Geochem. Geophs. Geosyst. 10, Q12014.
Cardenas, M.B., 2008. Three-dimensional vortices in single pores and their effects on transport. Geophys. Res. Lett. 35 (18).
Chaudhary, K., Cardenas, M., Deng, W., Bennett, P., 2013. Pore geometry effects on intrapore viscous to inertial flows and on effective hydraulic parameters. Water Resour. Res. 49, 1149–1162.
Chaudhary, K., Cardenas, M.B., Deng, W., Bennett, P.C., 2011. The role of eddies inside pores in the transition from Darcy to Forchheimer flows. Geophys. Res. Lett. 38 (24).
Comolli, A., Dentz, M., 2017. Anomalous dispersion in correlated porous media: a coupled continuous time random walk approach. Eur. Phys. J. B 90 (9), 166.
Cortis, A., Berkowitz, B., 2004. Anomalous transport in “classical” soil and sand columns. Soil Sci. Soc. Am. J. 68 (5), 1539–1548.
Davit, Y., Wood, B.D., Debenest, G., Quintard, M., 2012. Correspondence between one- and two-equation models for solute transport in two-region heterogeneous porous media. Transp. Porous Media 95 (1), 213–238.
De Anna, P., Le Borgne, T., Dentz, M., Tartakovsky, A.M., Bolster, D., Davy, P., 2013. Flow intermittency, dispersion, and correlated continuous time random walks in porous media. Phys. Rev. Lett. 110 (18), 184502.
Dentz, M., Cortis, A., Scher, H., Berkowitz, B., 2004. Time behavior of solute transport in heterogeneous media: transition from anomalous to normal transport. Adv. Water Resour. 27 (2), 155–173.
Dentz, M., Kang, P.K., Comolli, A., Le Borgne, T., Lester, D.R., 2016. Continuous time random walks for the evolution of lagrangian velocities. Phys. Rev. Fluids 1 (7), 074004.
Dykaar, B., Kitanidis, P., 1996. Macrotransport of a biologically reacting solute through porous media. Water Resour. Res. 32, 307–329.
Edery, Y., Guadagnini, A., Scher, H., Berkowitz, B., 2014. Origins of anomalous transport in heterogeneous media: structural and dynamic controls. Water Resour. Res. 50 (2), 1490–1505.
Harvey, C., Gorelick, S.M., 2000. Rate-limited mass transfer or macrodispersion: which dominates plume evolution at the macrodispersion experiment (MADE) site? Water Resour. Res. 36 (3), 637–650.
Hornung, U., 1997. Homogenization and Porous Media. Springer.
Iliev, O., Lakdawala, Z., Neßler, K., Prill, T., Vutov, Y., Yang, Y., Yao, J., 2017. On the pore-scale modeling and simulation of reactive transport in 3d geometries. Math. Model. Anal. 22 (5), 671–694. https://doi.org/10.3846/13926292.2017.1356759.
Kang, P.K., Dentz, M., Le Borgne, T., Juanes, R., 2011. Spatial Markov model of anomalous transport through random lattice networks. Phys. Rev. Lett. 107 (18), 180602.
Kang, P.K., Anna, P., Nunes, J.P., Bijeljic, B., Blunt, M.J., Juanes, R., 2014. Pore-scale intermittent velocity structure underpinning anomalous transport through 3-d porous media. Geophys. Res. Lett. 41 (17), 6184–6190.
Kang, P.K., Brown, S., Juanes, R., 2016. Emergence of anomalous transport in stressed rough fractures. Earth Planet. Sci. Lett. 454, 46–54.
Kang, P.K., Dentz, M., Le Borgne, T., Lee, S., Juanes, R., 2017. Anomalous transport in disordered fracture networks: spatial Markov model for dispersion with variable injection modes. Adv. Water Resour. 106, 80–94.
Kang, P.K., Le Borgne, T., Dentz, M., Bour, O., Juanes, R., 2015. Impact of velocity correlation and distribution on transport in fractured media: field evidence and theoretical model. Water Resour. Res. 51, 940–959. https://doi.org/10.1002/2014WR015799.
Khan, M., 1962. Non-equilibrium theory of capillary columns and the effect of interfacial resistance on column efficiency. Gas Chromatogr. 3–17.
Kitanidis, P., Dykaar, B., 1997. Stokes flow in a slowly varying two-dimensional periodic pore. Transp. Porous Media 26, 89–98.
Le Borgne, T.L., Dentz, M., Carrera, J., 2008a. Lagrangian statistical model for transport in highly heterogeneous velocity fields. Phys. Rev. Lett. 101, 090601.
Le Borgne, T., Dentz, M., Carrera, J., 2008b. Spatial Markov processes for modeling Lagrangian particle dynamics in heterogeneous porous media. Phys. Rev. E 78, 026308.
Le Borgne, T., Bolster, D., Dentz, M., Anna, P., Tartakovsky, A., 2011. Effective pore-scale dispersion upscaling with a correlated continuous time random walk approach. Water Resour. Res. 47 (12). https://doi.org/10.1029/2011WR010457. (W12538).
Le Borgne, T., Bolster, D., Dentz, M., de Anna, P., Tartakovsky, A., 2012. Effective pore-scale dispersion upscaling with a correlated CTRW approach. Water Resour. Res. 47, W12538.
Lester, D., Metcalfe, G., Trefry, M., 2014. Anomalous transport and chaotic advection in homogeneous porous media. Phys. Rev. E 90 (6), 063012.
Levesque, M., Bénichou, O., Voituriez, R., Rotenberg, B., 2012. Taylor dispersion with adsorption and desorption. Phys. Rev. E 86 (3), 036316.
da Luz, C., de Arruda Guelli Ulson de Souza, S., Ulson de Souza, A., Dervanoski, A., de Oliveira Samel Moraes, A., Wood, B., 2018. A multiscale model for carbon adsorption of btx compounds: comparison of volume averaging theory and experimental measurements. Chem. Eng. Sci. 184, 285–308. https://doi.org/10.1016/j.ces.2018.02.047.
Maghrebi, M., Jankovic, I., Allen-King, R.M., Rabideau, A.J., Kalinovich, I., Weissmann, G.S., 2014. Impacts of transport mechanisms and plume history on tailing of sorbing plumes in heterogeneous porous formations. Adv. Water Resour. 73, 123–133.
Maghrebi, M., Jankovic, I., Weissmann, G.S., Matott, L.S., Allen-King, R.M., Rabideau, A.J., 2015. Contaminant tailing in highly heterogeneous porous formations: sensitivity on model selection and material properties. J. Hydrol. 531, 149–160.
Massoudieh, A., Dentz, M., Alikhani, J., 2017. A spatial Markov model for the evolution of the joint distribution of groundwater age, arrival time, and velocity in heterogeneous media. Water Resour. Res. 53 (7), 5495–5515.
Morales, V.L., Dentz, M., Willmann, M., Holzner, M., 2017. Stochastic dynamics of intermittent pore-scale particle motion in three-dimensional porous media: experiments and theory. Geophys. Res. Lett. 44 (18), 9361–9371.
Most, S., 2019. Analysis and simulation of anomalous transport in porous media, Ph.D. thesis. In: University of Stuttgart.
Plumb, O., Whitaker, S., 1988. Dispersion in heterogeneous porous media: 1. Local volume averaging and large-scale averaging. Water Resour. Res. 24, 913–926.
Porta, G., Ceriotti, G., Thovert, J.-F., 2016. Comparative assessment of continuum-scale models of bimolecular reactive transport in porous media under pre-asymptotic conditions. J. Contam. Hydrol. 185, 1–13.
Porter, M.L., Valdés-Parada, F.J., Wood, B.D., 2010. Comparison of theory and experiments for dispersion in homogeneous porous media. Adv. Water Resour. 33 (9), 1043–1052.
Ptak, T., Teutsch, G., 1994. Forced and natural gradient tracer tests in a highly heterogeneous porous aquifer: instrumentation and measurements. J. Hydrol. 159 (1–4), 79–104.
Rathi, B., Neidhardt, H., Berg, M., Siade, A., Prommer, H., 2017. Processes governing arsenic retardation on pleistocene sediments: adsorption experiments and model-based analysis. Water Resour. Res. 53 (5), 4344–4360. https://doi.org/10.1002/2017WR020551.
Rehfeldt, K., Boggs, J., Gelhar, L., 1992. Field study of dispersion in a heterogeneous aquifer. 3: geostatistical analysis of hydraulic conductivity. Water Resour. Res. 28, 3309–3324.
Richmond, M.C., Perkins, W.A., Scheibe, T.D., Lambert, A., Wood, B.D., 2013. Flow and axial dispersion in a sinusoidal-walled tube: effects of inertial and unsteady flows. Adv. Water Resour. 62, 215–226 (Part B).
Risken, H., 1984. Fokker-Planck Equation. Springer.
Salles, J., Thovert, J.-F., Delannay, R., Prevors, L., Auriault, J.-L., Adler, P., 1992. Taylor dispersion in porous media. Determination of the dispersion tensor. Phys. Fluids A 5 (10), 2348–2376.
Seetha, N., Kumar, M. Mohan, Majid Hassanizadeh, S., Raoof, A., 2014. Virus-sized colloid transport in a single pore: model development and sensitivity analysis. J. Contam. Hydrol. 164, 163–180. https://doi.org/10.1016/j.jconhyd.2014.05.010.
Shapiro, M., Brenner, H., 1988. Dispersion of a chemically reactive solute in a spatially periodic model of a porous medium. Chem. Eng. Sci. 43 (3), 551–571.
Sherman, T., Fakhari, A., Miller, S., Singha, K., Bolster, D., 2017. Parameterizing the spatial markov model from breakthrough curve data alone. Water Resour. Res. 53 (12), 10888–10898.
Sherman, T., Foster, A., Bolster, D., Singha, K., 2018. Predicting downstream concentration histories from upstream data in column experiments. Water Resour. Res (Under Review).
Sund, N., Bolster, D., Mattis, S., Dawson, C., 2015a. Pre-asymptotic transport upscaling in inertial and unsteady flows through porous media. Transp. Porous Media 109 (2), 411–432.
Sund, N.L., Bolster, D., Dawson, C., 2015b. Upscaling transport of a reacting solute through a peridocially converging–diverging channel at pre-asymptotic times. J. Contam. Hydrol. 182, 1–15.
Sund, N.L., Bolster, D., Benson, D.A., 2016. Testing the limits of the spatial Markov model for upscaling transport: the role of nonmonotonic effective velocity autocorrelations. Phys. Rev. E 94 (4), 043107.
Sund, N., Porta, G., Bolster, D., Parashar, R., 2017a. A lagrangian transport eulerian reaction spatial (laters) Markov model for prediction of effective bimolecular reactive transport. Water Resour. Res. 53 (11), 9040–9058.
Sund, N.L., Porta, G.M., Bolster, D., 2017b. Upscaling of dilution and mixing using a trajectory based spatial markov random walk model in a periodic flow domain. Adv. Water Resour. 103, 76–85.
Taylor, G., 1953. Dispersion of soluble matter in solvent flowing slowly through a tube. Proc. R. Soc. Lond. Ser. A 219, 186–203 186–203.
Wright, E., Sund, N., Richter, D., Porta, G., Bolster, D., 2019. Upscaling mixing in highly heterogeneous porous media via a spatial markov model. Water 11 (1), 53.
Zhang, Y., Benson, D.A., Baeumer, B., 2007. Predicting the tails of breakthrough curves in regional-scale alluvial systems. Groundwater 45 (4), 473–484.
Zhang, L., Hesse, M.A., Wang, M., 2017. Transient solute transport with sorption in poiseuille flow. J. Fluid Mech. 828, 733–752. https://doi.org/10.1017/jfm.2017.546.